Available online at www.sciencedirect.com

ScienceDirect

Ceramics International 40 (2014) 3939–3946

CERAMICS INTERNATIONAL

www.elsevier.com/locate/ceramint

Optimization of binder removal for ceramic microfabrication via polymer co-extrusion

Khurshida Sharmin, Ingmar Schoegl*

Department of Mechanical and Industrial Engineering, Louisiana State University, Baton Rouge, LA 70803, USA

Received 17 July 2013; received in revised form 7 August 2013; accepted 8 August 2013
Available online 16 August 2013

Abstract

The objective of this study is to assess the feasibility of solvent extraction (SE) for partial binder removal in the context of polymer co-extrusion with a thermoplastic binder component. Polymer co-extrusion is able to produce multilayered, functionally graded and/or textured structures in an efficient manufacturing process, but requires a polymer binder system with suitable flow characteristics. Traditionally, the binder is removed by thermal debinding (TD), which, however, is prone to form cracks or blisters, both of which are attributed to a lack of initial pore space that allows pyrolysis products to escape. The primary focus of this work is to demonstrate that a binder system with a high soluble binder content is suitable for conventional polymer co-extrusion and to document that a two-step binder removal process involving both SE and TD eliminates debinding defects. The overall fabrication process is documented for the extrusion of solid ceramic rods and co-extrusion of tubes, where alumina powder was batched with polyethylene butyl acrylate (PEBA) as backbone polymer and polyethylene glycol (PEG) as water soluble binder. SE for specimen with varying PEBA:PEG ratios was tested in water at three different temperatures for various times. The 1:1 mixture showed a PEG removal up to 80 wt.% of the original PEG content after 6 h extraction; after subsequent thermal debinding, rods and tubes sintered successfully without defects, demonstrating the viability of the process.

Keywords: A. Sintering; B. Defects; D. Al_2O_3; Solvent extraction

1. Introduction

Co-extrusion of thermoplastic compounds loaded with ceramic powders is a cost effective and promising method for manufacturing multilayered, functionally graded, or textured structures. By simultaneous extrusion of a feedrod assembled from multiple materials, diphasic or multilayered structures are easily fabricated. In the available literature, there are two different types of binder systems used for co-extrusion: (i) thermoplastic polymers [1–4] and (ii) waxes and/or starches [5,6], where in either case the binder system requires suitable rheological characteristics to achieve accurate shape reduction during co-extrusion. Thermoplastic binders facilitate the fabrication of intricate structures, and the construction of micron-scaled structures using multiple passes with increasingly complex feedrods is well documented [1,2,4]. Most studies with thermoplastic binders, however, focus on the fabrication of green bodies: despite added complexity of the burn-out process, debinding and sintering steps are often not addressed in detail. Commonly used polymer binders include EVA (ethylene vinyl acetate) [2,7], EEA (ethylene ethyl acrylate) [1,8–10], PEBA (polyethylene butyl acrylate) [11–13], and LDPE (low density polyethylene) [14]. Due to the lack of a soluble binder component, the documented polymer binder mixtures require thermal debinding (TD) with exceedingly low heating rates and carefully selected heating schedules, as they are prone to form cracks or blisters during debinding [1,13,14].

Since the late 1990s, a range of studies have been conducted on microfabrication based on co-extrusion of ceramic materials using thermoplastic binder systems. The fabrication process involves three fundamental issues, (a) similar rheology for dissimilar materials to ensure successful extrusion, (b) binder removal without damaging the specimen, and (c) matched

*Corresponding author. Tel.: +1 2255784332.
E-mail addresses: ksharm5@tigers.lsu.edu (K. Sharmin), ischoegl@lsu.edu (I. Schoegl).

0272-8842/$ - see front matter © 2013 Elsevier Ltd and Techna Group S.r.l. All rights reserved.
http://dx.doi.org/10.1016/j.ceramint.2013.08.039

densification for co-sintering. Ismael et al. investigated the flow characteristics for co-extrusion and successfully done with the similar flow property between lead zirconate titanate/low density polyethylene (LDPE) and carbon/LDPE mixtures [14]. Xu and Hilmas studied the viscosity of pure polymer melts and ceramic/polymer mixtures for rheology control in the co-extrusion process [11]. In addition to binder systems that involve thermoplastic polymers, the importance of matched rheologies in the context of co-extrusion has been documented for conventional pastes [5,6]. Once co-extruded samples are obtained, conventional TD is commonly suggested for binder removal. In TD, the initial step involves the decomposition of polymeric additives into gaseous species [15], where non-trivial chemical interactions between mixture components have been documented [10]. Gaseous decomposition products formed in the interior of the sample have to diffuse to the sample surface. If the escaping rate from the sample is not sufficiently high, vapor nuclei are formed that grow into bubbles and result in bubbling and bloating [16–18]. Defects originating in the debinding process can be attributed to a lack of initial pore space for outgassing of pyrolysis products. Another source of defects is co-sintering of dissimilar materials, where a mismatch of sintering shrinkage percentages and sintering temperatures can cause slumping or interface instabilities [2].

Co-extrusion with thermoplastic binder systems involves batching of mixtures, construction of a feedrod, extrusion, debinding and sintering. A comparison to other ceramic forming technologies reveals some similarities to powder injection molding (PIM), despite having significant differences in the forming steps with associated differences in binder rheologies. In the context of PIM, debinding processes and elimination of debinding defects have been documented in detail. Using conventional TD, improvements have been achieved by controlling the debinding schedule and heating rate [19], using inert atmosphere to minimize the oxidation [17], placing samples on powdered bed to wick liquefied binders through interconnected pores [18] or using a low molecular weight binder with low boiling point to initiate pores at an early stage of TD [20]. As an alternative to TD, solvent extraction (SE) uses a binder component that is soluble and can be removed. Solvent extraction is a two-stage process consisting of dissolution and diffusion [21,22]. Once the samples are immersed in a suitable solvent, the soluble binders start to incorporate solvent into a swollen gel, which starts to dissolve once the solvent concentration is sufficiently large [23]. This partial removal of the binder creates pore space and as the debinding time increases, the pore spaces are expanding to the inner region of the samples. A combination of SE and TD has been proven to be an efficient approach to eliminate defects [19,24]. Pore space created during the initial SE step allows pyrolysis gases to escape during subsequent TD, and thus lead to a reduction of cracks [22,25]. Studies on combining SE using PEG as soluble binder with TD reported crack free samples [26,27] and reduced debinding times [19]. It has, however, been shown that cracks or blistering can be caused by swelling of PEG, especially at higher temperature and for high molecular weights [28]. Zaky and Lin et. al reported the swelling effect at 60 °C for different binder systems (wax and SA) [29,30]. When different combinations of low and high molecular weight of PEG were used as soluble binders, it was observed that binders containing high molecular weight of PEG (6000, 8000) can cause the defects even at temperatures as low as 30 °C, 40 °C, and 50 °C [24,28]. Using low to medium molecular weight PEG (400, 600, 1000, 1500, 3350) as water soluble binders, no swelling was reported [26,27]. It was suggested that the combination of low and high molecular weight of PEG yielded no swelling effect up to 50 °C [24,31].

The present work seeks to demonstrate the feasibility of a combined SE/TD debinding process for a binder system that is suitable for polymer co-extrusion. A thermoplastic binder backbone (PEBA) and a water soluble binder component (PEG) are used for the extrusion of solid alumina rods and co-extrusion of alumina tubes. A conventional PEBA mixture without soluble components was used as a control. The combined SE/TD debinding process was investigated for varying PEBA:PEG ratios, solvent temperatures and debinding atmospheres. Defects were studied for both green and sintered specimen.

2. Experimental procedure

Ceramic rods and tubes with water soluble binder components were fabricated by (co-)extrusion. All results are documented for 5.84 mm diameter samples.

Materials and batching. Alpha alumina powder (Al_2O_3, Informat Advanced Materials) with particle size 150 nm was used for all ceramic/binder mixtures. For the preparation of carbon cores for co-extrusion, carbon black BP 120 (Cabot Corporation) was used instead of alumina. The binder system consists of PEBA to maintain green strength, and PEG as water soluble binder. PEBA (Lotryl 35-BA-40, Arkema Inc.) is a random copolymer of ethylene and butyl acrylate containing 33–37% butyl acrylate with an overall melt index of 35–45. Two molecular weights of PEG were used in this work: PEG6000 (Alfa Aesar) as binder and PEG200 (J.T. Baker) as plasticizer. For the control mixture without soluble component, heavy mineral oil (HMO, Fisher Scientific) was used as a plasticizer.

All the binder materials were batched with ceramic powder in a HAAKE Rheocord 90 (Rheomix 600) at 30 rpm and 130 °C. The ceramic powder loading was 55 vol.% to ensure densification [11]. The volume of the mixing chamber with roller rotors was 69 cc and 70% of the volume was filled during mixing. For batching, half of the alumina powder and half of PEG6000 were added simultaneously to the molten PEBA. The remaining alumina powder and PEG6000 were added slowly; the viscosity was adjusted using PEG200 before kneading the mixture for 25 min. All batches were processed twice to ensure homogeneous mixing. Table 1 lists the mixture compositions prepared for this study, where the PEG amount increased while PEBA was reduced.

Extrusion. Extrusions and co-extrusions were performed with a custom ram extruder constructed from on a 30 KN ComTen

Table 1
Compositions (vol.%) of all mixtures.

Mixture (PEBA:PEG)	Al_2O_3	Carbon	PEBA	PEG6000	PEG200	HMO	Barrel Temp. (°C)	Die Temp. (°C)
Ceramic Mix1 (1:0)	55.35	–	40.78	–	–	3.88	130	135
Ceramic Mix2 (2:1)	55.37	–	29.29	11.84	3.50	–	115	120
Ceramic Mix3 (1:1)	55.68	–	22.09	18.71	3.52	–	110	115
Ceramic Mix4 (1:2)	55.52	–	14.68	26.29	3.51	–	105	110
Carbon Core (1:1)	–	50.52	24.96	21.03	3.51	–	110	115

Universal Tester (95TL5K), where a barrel of 133 mm length and 19 mm diameter is mounted in a compression frame. A hyperbolic shaped die of 5.84 mm diameter was attached to the ram extruder resulting in a size reduction of 10.5:1. Two band heaters were used in the barrel and in the die region to control the temperature during extrusion. Feedrods were pressed into cylinders prior to extrusion. For co-extrusion, feedrods were manufactured by inserting extruded carbon core material into holes drilled into cylindrical feedrods. Extrusions were carried out at a fixed ram speed of 7.62 mm/min, where temperatures are listed in Table 1.

Solvent extraction. SE was performed by immersing the samples in a water bath in a controlled temperature environment. To investigate the effect of temperature and extraction time on PEG removal, tests were performed by changing the water temperature from room temperature to 45 °C and extraction times ranging from 1 to 6 h. After extraction, the samples were dried at room temperature and PEG weight loss was calculated as a percentage of the original PEG content. For each solvent extraction condition, five samples were obtained and the average PEG loss was documented. Measurement uncertainties were calculated by a Student-t distribution. PEG loss data was also verified by TGA tests under N_2 atmosphere with a ramping rate of 2.5 °C/min to 800 °C. In order to verify that solvent extraction creates pore space, extracted Mix3 (1:1) samples were again immersed in water and the wet weight was recorded. Results for pore space volume calculated from PEG loss and water incorporation matched within 5%, where the small discrepancy is attributed to incomplete permeation and/or minor swelling of residual PEG.

Thermal debinding and Sintering. TD was performed in a Lindberg Blue M tube furnace with a heating rate of 1.25 °C/min to 1000 °C. Although TGA shows that all the binder was removed at 600 °C, heating was continued to a higher temperature to initiate pre-sintering. To prevent the formation of cracks, TD was carried out in two stages with N_2 and air, respectively: the inert N_2 atmosphere minimizes the rate of oxidation reactions, and subsequent heating in air removes remaining carbon from the sample. After debinding, samples were sintered at 1600 °C for 1 h in a 1800 MTI high temperature furnace.

Optical and scanning electron microscopy. Sample morphologies were studied for both green and sintered specimen. Optical micrographs (LEICA MZ75) are used to illustrate the shrinking core during SE and cracks found after debinding. ImageJ [32] software was used to measure the core radius during SE, where a measurement uncertainty of 20% was assumed. Details on the microstructure of green and sintered specimen were investigated using a scanning electron microscope (SEM) (*FEI*™, Quanta 3D FEG).

3. Results and discussion

3.1. Microscopy on solvent extracted sample

The binder was removed in three steps: (i) solvent extraction (SE) to initiate interstitial pore space, (ii) thermal debinding in N_2 (TD_{N_2}) to promote pyrolysis of organic binders and (iii) thermal debinding in air (TD_{air}) to remove carbon residues. In addition to tests with PEBA:PEG mixtures, a control mixture without PEG component (Mix1; PEBA:PEG = 1:0) was subjected to a 2-stage TD to investigate the impact of PEG. For SE, 25.4 mm long extruded rod samples were immersed in water at room temperature (RT), 35 °C and 45 °C, for durations ranging from 1 to 6 h. During solvent extraction, a clearly visible boundary between an outer shell where PEG has been removed and an inner core with undissolved PEG was observed. As the extraction time increased, the radius of the undissolved core decreased, as shown in Fig. 1. A comparison of extraction for Mix3 (1:1) and Mix2 (2:1) at 35 °C showed a significantly faster core removal for the sample with higher PEG content: for Mix3 (1:1), no visible core remains after 2 h, while for Mix2 (2:1), a small core is still visible after 6 h. The occurrence of a moving boundary is consistent with the previous studies on solvent extraction [22,33].

Fig. 2 shows the cross-sectional SEM images for Mix2 (2:1) after 4 h SE extraction. For the core region, Fig. 2a demonstrates that there is no pore or void space as undissolved PEG is still present in this region. At the interface (Fig. 2b), small pores between strands of polymer binder are apparent. The more PEG was extracted at the outer shell area, the more void spaces or pores were formed (Fig. 2c). During thermal debinding, these pores allow the pyrolysis products to escape from the sample.

The microstructure of the alumina-PEBA-PEG blend plays a major role in the success of solvent extraction. Tests with an unfilled PEBA/PEG mixture reveal that PEBA and PEG do not mix and remain phase separated. While filler material enforces dispersion of the phases throughout the mixture, phase separation of PEBA and PEG will persist at the microscale, which is expected to form a three-phase mixture. According to percolation theory [34], contiguous PEG regions exist as long as a sufficient volume percentage of PEG is present. After solvent extraction, a PEBA-alumina network with contiguous

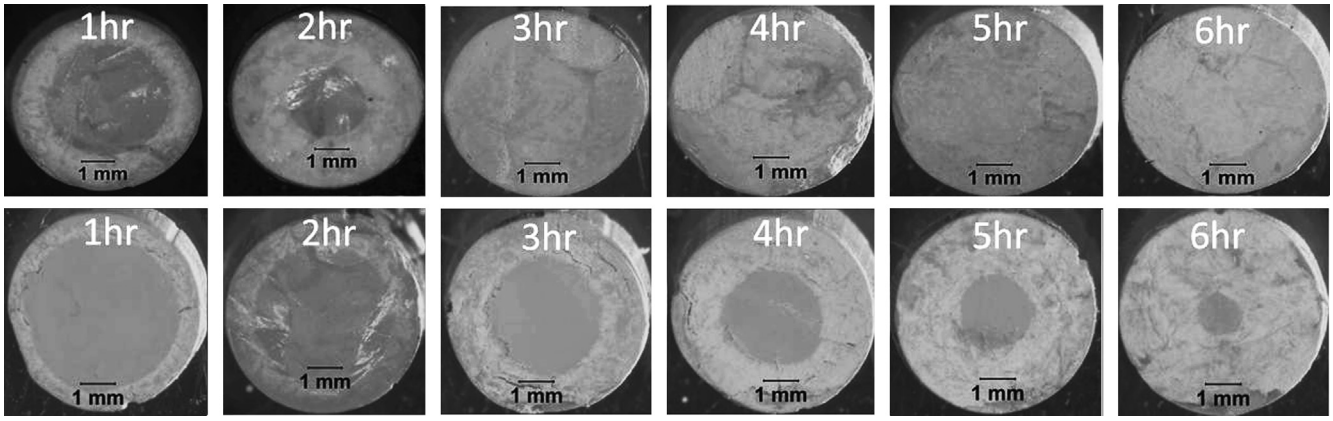

Fig. 1. Cross-sectional views of rods as a function of solvent extraction time at 35 °C; top and bottom rows illustrate the evolution of a shrinking core for Mix3 (1:1) and Mix2 (2:1), respectively. The lighter area (shell) represents the region from which PEG was extracted, and the dark area (core) contains undissolved PEG. Samples were cut with a razor blade.

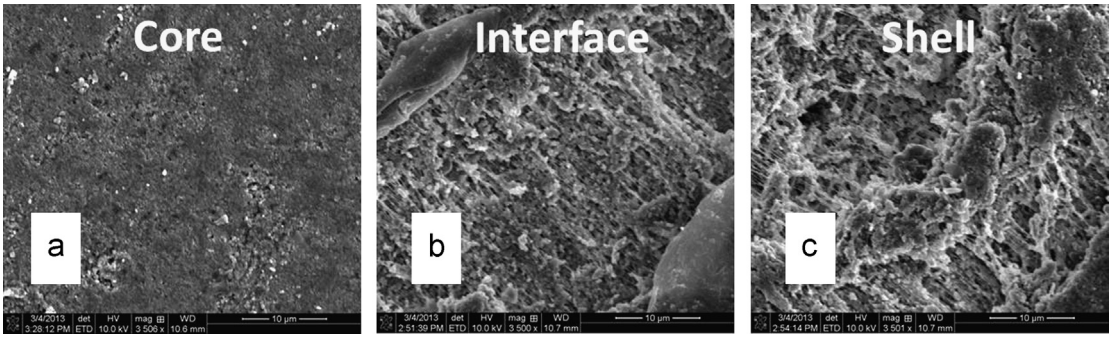

Fig. 2. SEM images of cross-sections formed by razor blade cuts after 4 h solvent extraction at 35 °C for Mix2 (2:1) samples: (a) core, (b) interface, and (c) shell.

pore space remains, which is corroborated by the SEM images shown in Fig. 2b and c.

3.2. PEG extraction with time and temperature

Fig. 3 shows measurements of the core radius for Mix2 (2:1) as a function of extraction time and water temperature. Specimen subjected to extraction at RT and 35 °C had cores up to 6 h and at 45 °C up to 4 h. Samples maintained the shape during extraction and showed good structural integrity after drying. Tests with Mix4 (1:2) formed an exception, where swelling was observed after 2 h of extraction, and material strength was insufficient for further processing after PEG removal. Compared to all other mixtures, Mix4 (1:2) has the smallest amount of thermoplastic backbone binder; swelling stress increased the volume of samples, which is a documented process for crack formation [24].

Further information on PEG removal was obtained by comparing sample weights before and after extraction. Fig. 4a shows the effect of solvent extraction time on the PEG removal at 45 °C. As expected, the percentages of PEG removal increased with time for all mixtures, where Mix3 (1:1) showed 80 wt.% of PEG removal after 6 h extraction, which is comparable to PEG removal reported in the literature [21,24,35]. Likewise, results show higher PEG removal rates for mixtures with higher PEG content at comparable extraction times, which is due to the effect of increased

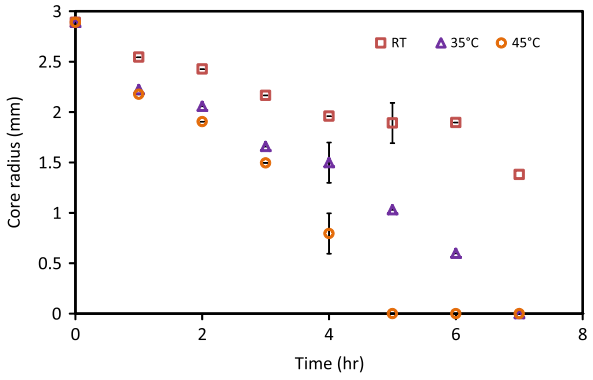

Fig. 3. Impact of time and solvent temperature on radius of undissolved core – Mix2 (2:1).

porosity formed by the larger amount of PEG in the mixture. A comparison of results for weight loss and core radius reveal that the core vanishes when a sample lost approximately 50 wt.% of PEG. The effects of temperature on PEG loss are shown in Fig. 4b for Mix2 (2:1). In analogy to results for core shrinkage, the rate of PEG removal is observed to increase as the temperature is raised from RT to 45 °C. At higher temperature, PEG dissolving is promoted due to an increase of the solubility of PEG in water [19,24]. The amount of lost PEG was verified by TGA tests shown in Fig. 5.

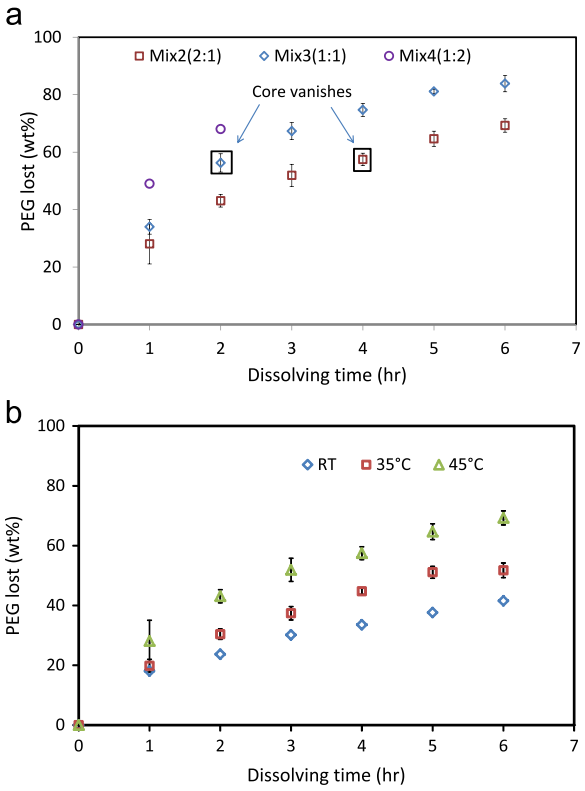

Fig. 4. PEG loss of ceramic samples as a function of extraction time: (a) comparison of different mixtures at a solvent temperature of 45 °C and (b) effect of solvent temperature on SE for Mix2 (2:1).

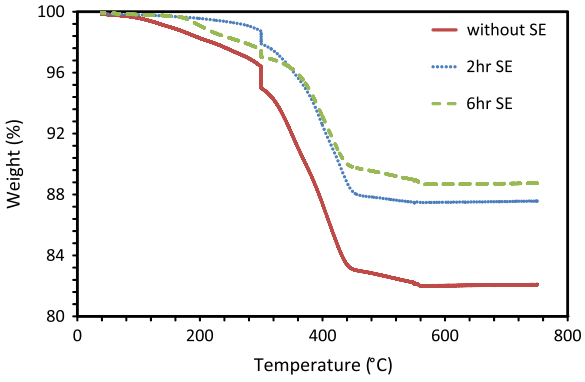

Fig. 5. TGA analysis of Mix3 (1:1) in N_2 atmosphere with and without SE at 45 °C.

3.3. Thermal debinding and sintering

TGA test. The weight change during TD was evaluated using TGA (Fig. 5). Mix3 (1:1) decomposed in three steps where the first loss occurred in the temperature range of 80–250 °C due to the elimination of crystallization water. The second step of weight loss combined the decomposition of PEG [27,10] in the range of 300–410 °C and PEBA in the range of 250–520 °C. A sharp weight drop around 300 ° C is attributed to rapid volatization of PEG 200, whereas PEG with higher molecular weights decompose at higher temperatures over a broader range of temperatures [36]. In the third step, weight loss occurred due to carbon loss in air. In Fig. 5, sample 'a' (before SE), shows a total weight loss of about 17.67 wt.%, which is close to the total binder weight percentage of 17.45% in Mix3 (1:1). At the beginning (150–350 °C), sample 'c' (6 h SE) shows a faster weight loss than sample 'b' (2 h SE), which is attributed to a larger amount of open pores available for outgassing. In theory, PEG is removed by SE from sample 'c'. Minor discrepancies between theoretical and actual weight loss in the extracted sample are attributed to small amounts of residual PEG: even if the core is removed (Fig. 3), small amounts of PEG remain within the samples (Fig. 4).

Evaluation of thermal debinding. Several different debinding protocols were investigated for the mixtures as listed in Table 2. The control mixture without PEG, Mix1 (1:0), was run in both air and a sequence of inert gas (N_2) and air. Although the inclusion of TD in N_2 improved results, defects were found in both cases. Without N_2, cracking is attributed to excessively fast oxidation; in both cases, a lack of open pores initiates the formation of blisters (Fig. 6a) [17]. Samples of Mix2 (2:1), which contain PEG but were not subjected to solvent extraction, also showed defects when run in air and a combination of both atmospheres, although defects manifested themselves in cracks rather than blisters. The impact of solvent extraction on defects was evaluated for samples with 2, 4 and 6 h of SE at 45 °C. In all cases, samples had initial pores before TD was run in N_2 followed by air; an unextracted core was only present for the 2 h sample. After 2 h SE, cracks were still found as illustrated in Fig. 6b. As either of the 4 and 6 h SE sample of Mix2 (2:1) showed no defects (Fig. 6c), the initiation of cracks in the 2 h sample is attributed to the presence of an unextracted core. Tests were repeated for Mix3 (1:1) samples, which have a larger PEG content, and thus show increased PEG loss during SE. After SE, none of the 2, 4, and 6 h samples had an unextracted core; after TD in N_2 and air, samples showed no macroscopic defects or cracks. A final test for Mix3 (1:1) with 6 h of SE but no intermediate burnout in N_2 resulted in a cracked sample.

In order to investigate microscopic defects, SEM images were obtained at the center of sintered samples of Mix3 (1:1). Sintering was performed at 1600 °C for 1 h for all cases. Fig. 7a shows that microscopic cracks are present in the sample without SE, which is consistent with macroscopic cracks observed after TD. Although it did not show any macroscopic cracks after TD, Fig. 7b reveals microscopic defects at the center of a sintered 2h, extracted sample. Again, defects are attributed to insufficient initial pore space at the sample core due to insufficient PEG removal by SE. After 4 h SE, enough pores were formed throughout the sample which resulted in a defect-free sintered specimen (Fig. 7c).

3.4. Co-extrusion of ceramic tubes

Ceramic feedrods with carbon cores were successfully co-extruded, and results are illustrated in Fig. 8. Although some distortions were found in the shape of the carbon core, ceramic shells and carbon cores maintained the reduction ratio and

Table 2
Overview of debinding defects showing the impact of extraction time and debinding atmosphere.

Mixture (PEBA:PEG)	SE	TD1	TD2	Observations
Mix1 (1:0)	–	–	Air	Blisters, cracks
	–	N_2	Air	Blisters
Mix2 (2:1)	–	–	Air	Cracks
	–	N_2	Air	Cracks
	2 h	N_2	Air	Cracks
	4 h	N_2	Air	No defects
	6 h	N_2	Air	No defects
Mix3 (1:1)	2 h	N_2	Air	No defects
	4 h	N_2	Air	No defects
	6 h	N_2	Air	No defects
	6 h	–	Air	Cracks

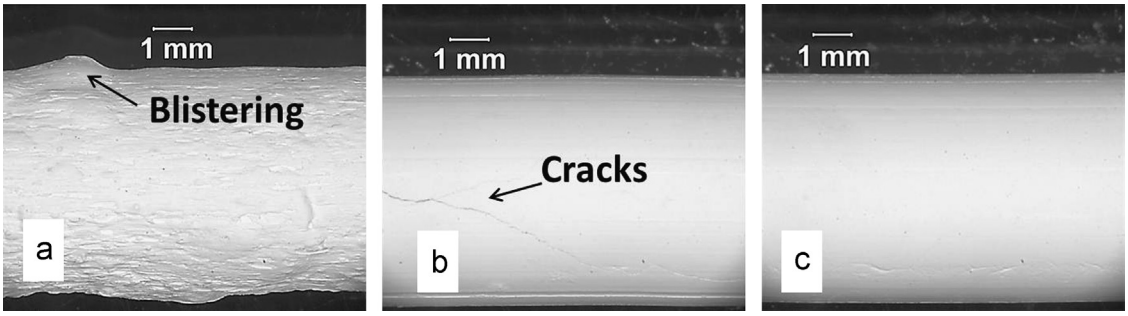

Fig. 6. Optical images after TD in N_2 and air showing the effect of SE on macroscopic defects: (a) Mix1 (1:0) – no SE , (b) Mix2 (2:1) after 2 h SE and (c) Mix2 (2:1) after 4 h SE.

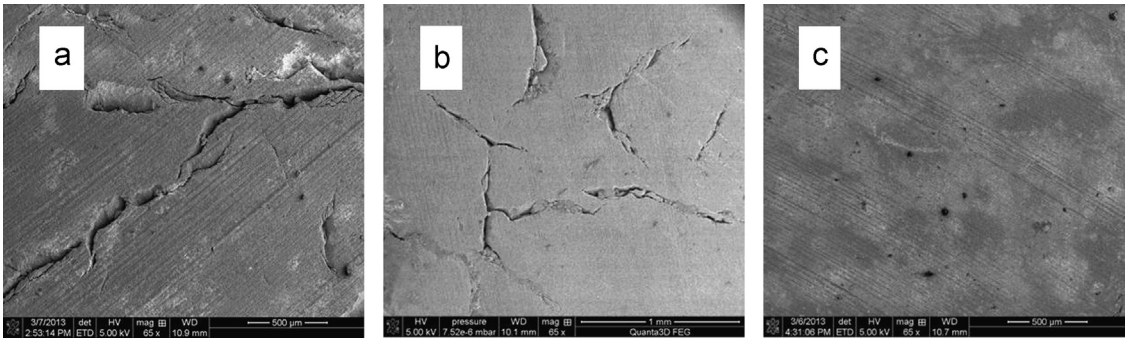

Fig. 7. SEM images of the sintered rod for Mix3 (1:1) illustrating the effect of SE duration: (a) without SE, (b) 2 h SE and (c) 4 h SE at 45 °C.

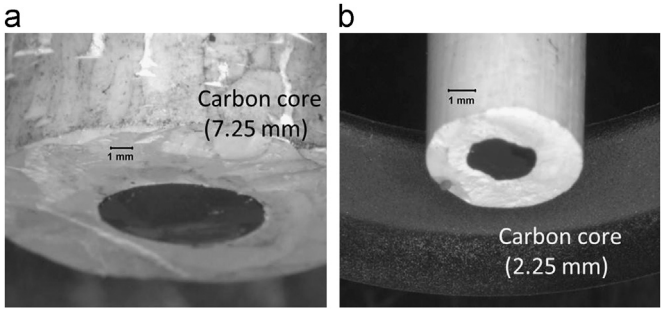

Fig. 8. Optical images of feedrod and co-extruded tube: (a) 19 mm feedrod with 7.2 mm core and (b) co-extruded tube with 5.84 mm diameter and a 2.2 mm core.

visual inspection did not reveal other defects. Fig. 8a shows the initial feedrod with a diameter of 19 mm, which consists of ceramic/binder as shell and carbon black/binder as core. The dimensions of the carbon cores reveal exact size reduction, i.e. in terms of area reduction, the extruded carbon core (2.2 mm) is 10.5 times smaller than the preform (7.2 mm), which is the same ratio as feedrod diameter (19 mm) to die diameter (5.84 mm). Co-extruded tubes from Mix2 (2:1) and Mix3 (1:1) were subjected to SE at the same three temperatures as the solid ceramic rods and the result showed that PEG removal percentages were analogous to the PEG removal from solid rods: after 6 h, solvent extraction removed ~70% of PEG in Mix2 (2:1) and ~80% of PEG in Mix3 (1:1)

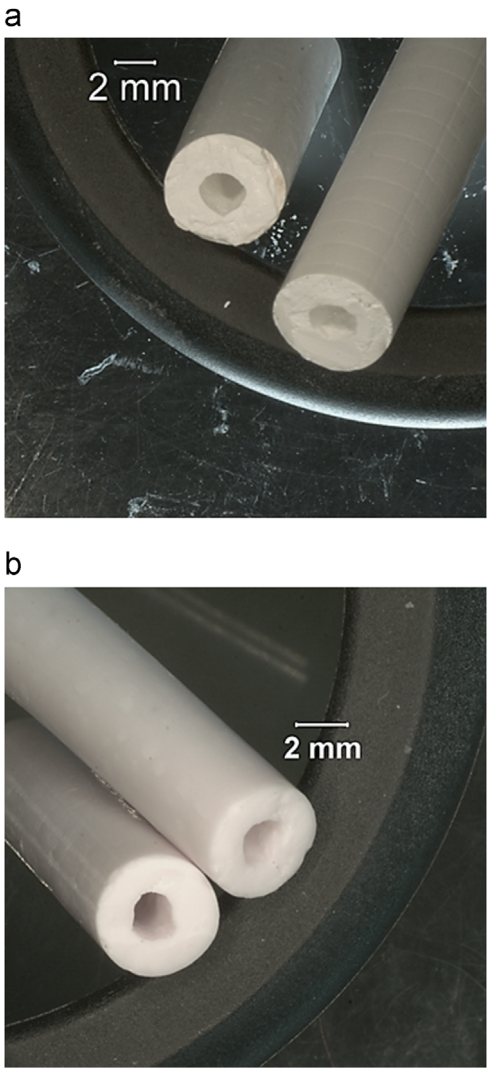

Fig. 9. Optical images of co-extruded tubes of Mix3 (1:1): (a) after 6 h SE followed by TD in N_2 and air and (b) after sintering.

Optical images of co-extruded samples after burn-out and final sintering are shown in Fig. 9. After burn-out, the binders were completely removed and a central hole remained after oxidation of the carbon core. The sintered sample was reduced uniformly from the original green sample and fully sintered (Fig. 9b). In all cases, detailed images showed neither macroscopic nor microscopic defects.

4. Conclusions

A complete processing route for co-extrusion and debinding of ceramic samples with a thermoplastic binder was investigated, where PEG was added to the binder system to allow for solvent extraction. Tests involved alumina rods and tubes, which were fabricated using a ram extruder. Binder removal involved a combination of solvent extraction (SE) with thermal debinding (TD) in N_2 and air, after which samples were sintered to full density. During solvent extraction, a moving boundary between unextracted core and extracted shell was clearly visible, where SEM images revealed interconnected void spaces in the extracted area. PEG removal increased with extraction time, and was accelerated by elevated temperature or increased PEG content within the mixture. Excessive amounts of PEG content led to a loss of green strength, where swelling was observed. A mixture with equal amounts of PEBA and PEG, – Mix3 (1:1), – showed good PEG removal, with 80 wt.% after 6 h extraction at 45 °C.

Results of the study demonstrate that debinding defects are eliminated by two measures: (a) contiguous interstitial pore space created by solvent extraction allows for outgassing of products during thermal debinding, and (b) an initially inert atmosphere during thermal debinding promotes break-down of organic binders via pyrolysis rather than oxidation. Tests with PEBA:PEG mixtures showed that both measures are necessary for defect-free samples; residual carbon is removed with a second burnout step in air prior to sintering. While the study focused on the optimization of binder removal to eliminate debinding defects, the rheology of the PEBA:PEG mixtures was satisfactory and co-extrusion of tubes was successful. As the creation of pore space forms the critical step, it is expected that a combined SE/TD debinding protocol will be successful for alternative thermoplastic binder systems as long as a soluble binder component allows for solvent extraction.

Acknowledgments

This work was partially funded by the LSU/CoE Fund for Innovation in Energy Research (FIER). We would like to thank Dr. Ioan Negulescu for giving access to a torque rheometer for mixture batching, Dr. Rafael Cueto for assistance with TGA, and Dr. Shengmin Guo for access to a sintering furnace. Dr. Desiderio Kovar and Dr. James Mikulak at UT Austin provided critical insights for the extrusion process. We also thank undergraduate students Tyler Lollis, AJ Pisano and Marcus Vasquez for assistance in batch mixing and preparation of the paper. In addition, Cabot corporation and Arkema Inc. are acknowledged for providing materials.

References

[1] Y.-H. Koh, H.-W. Kim, H.-E. Kim, J.W. Halloran, Fabrication of macrochannelled-hydroxyapatite bioceramic by a coextrusion process, Journal of the American Ceramic Society 85 (10) (2002) 2578–2580.
[2] C.V. Hoy, A. Barda, M. Griffith, J.W. Halloran, Microfabrication of ceramics by co-extrusion, Journal of the American Ceramic Society 81 (1) (1998) 152–158.
[3] M. Trunec, Fabrication of zirconia-and ceria-based thin-wall tubes by thermoplastic extrusion, Journal of the European Ceramic Society 24 (4) (2004) 645–651.
[4] D. Kovar, B.H. King, R.W. Trice, J.W. Halloran, Fibrous monolithic ceramics, Journal of the American Ceramic Society 80 (10) (1997) 2471–2487.
[5] R. Greenwood, K. Kendall, O. Bellon, A method for making alumina fibres by co-extrusion of an alumina and starch paste, Journal of the European Ceramic Society 21 (4) (2001) 507–513.
[6] C. Kaya, E. Butler, M. Lewis, Co-extrusion of Al_2O_3/ZrO_2 bi-phase high temperature ceramics with fine scale aligned microstructures, Journal of the European Ceramic Society 23 (6) (2003) 935–942.
[7] B.-T. Lee, A. Esfakur Rahman, J.-H. Kim, Novel design of microchanneled tubular solid oxide fuel cells and synthesis using a multipass

extrusion process, Journal of the American Ceramic Society 90 (6) (2007) 1921–1925.
[8] J.-J. Sun, Y.-H. Koh, W.-Y. Choi, H.-E. Kim, Fabrication and characterization of thin and dense electrolyte-coated anode tube using thermoplastic coextrusion, Journal of the American Ceramic Society 89 (5) (2006) 1713–1716.
[9] W.G. Fahrenholtz, G. Hilmas, A. Chamberlain, J. Zimmermann, Processing and characterization of ZrB2-based ultra-high temperature monolithic and fibrous monolithic ceramics, Journal of Materials Science 39 (19) (2004) 5951–5957.
[10] A.M. Knapp, J.W. Halloran, Binder removal from ceramic-filled thermoplastic blends, Journal of the American Ceramic Society 89 (9) (2006) 2776–2781.
[11] X. Xu, G. Hilmas, The rheological behavior of ceramic/polymer mixtures for coextrusion processing, Journal of Materials Science 42 (4) (2007) 1381–1387.
[12] D. Beeaff, G. Hilmas, Rheological behavior of coextruded multilayer architectures, Journal of Materials Science 37 (6) (2002) 1259–1264.
[13] L. Walker, J. Miller, G. Hilmas, L. Evans, E. Corral, Coextrusion of zirconia-iron oxide honeycomb substrates for solar-based thermochemical generation of carbon monoxide for renewable fuels, Energy and Fuels 26 (2012) 712–721.
[14] M. Ismael, F. Clemens, P. Wyss, T. Graule, M. Hoffmann, Processing, microstructure and electromechanical properties of $Pb(Zr, Ti)O_3$ fibers obtained by thermoplastic co-extrusion, in: 18th IEEE International Symposium on the Applications of Ferroelectrics, 2009 (ISAF 2009), IEEE, pp. 1–4.
[15] B.-Å. Sultan, E. Sörvik, Thermal degradation of eva and eba—a comparison. I. Volatile decomposition products, Journal of Applied Polymer Science 43 (9) (1991) 1737–1745.
[16] A. Oliveira, M. Kaviany, K. Hrdina, J. Halloran, Mass diffusion-controlled bubbling and optimum schedule of thermal degradation of polymeric binders in molded powders, International Journal of Heat and Mass Transfer 42 (17) (1999) 3307–3329.
[17] M. Trunec, J. Cihlar, Thermal debinding of injection moulded ceramics, Journal of the European Ceramic Society 17 (2) (1997) 203–209.
[18] W.J. Tseng, C.-K. Hsu, Cracking defect and porosity evolution during thermal debinding in ceramic injection moldings, Ceramics International 25 (5) (1999) 461–466.
[19] P. Thomas-Vielma, A. Cervera, B. Levenfeld, A. Várez, Production of alumina parts by powder injection molding with a binder system based on high density polyethylene, Journal of the European Ceramic Society 28 (4) (2008) 763–771.
[20] J. Zhou, B. Huang, E. Wu, Extrusion moulding of hard-metal powder using a novel binder system, Journal of Materials Processing Technology 137 (1) (2003) 21–24.
[21] S. Eroglu, H. Bakan, Solvent debinding kinetics and sintered properties of injection moulded 316l stainless steel powder, Powder Metallurgy 48 (4) (2005) 329–332.
[22] W.-W. Yang, K.-Y. Yang, M.-C. Wang, M.-H. Hon, Solvent debinding mechanism for alumina injection molded compacts with water-soluble binders, Ceramics International 29 (7) (2003) 745–756.
[23] K. Hwang, Y. Hsieh, Comparative study of pore structure evolution during solvent and thermal debinding of powder injection molded parts, Metallurgical and Materials transactions A 27 (2) (1996) 245–253.
[24] Y. Xianfeng, J. Cui, X. Zhipeng, L. Wei, L. Qicheng, Water-soluble binder system based on poly-methyl methacrylate and poly-ethylene glycol for injection molding of large-sized ceramic parts, International Journal of Applied Ceramic Technology 10 (2) (2013) 339–347.
[25] J. Cheng, L. Wan, Y. Cai, J. Zhu, P. Song, J. Dong, Fabrication of w–20 wt.% cu alloys by powder injection molding, Journal of Materials Processing Technology 210 (1) (2010) 137–142.
[26] S. Liang, B. Huang, Z.A. Ahmad, A.F. Mohd Noor, K. Hussin, Preparation and evaluation of Al_2O_3 plastic forming feedstock with partially water soluble polymer as a binder, Journal of Materials Processing Technology 137 (1) (2003) 128–131.
[27] Y. Thomas, B.R. Marple, Partially water-soluble binder formulation for injection molding submicrometer zirconia, Advanced Performance Materials 5 (1–2) (1998) 25–41.
[28] M. Song, M.S. Park, J.K. Kim, I.B. Cho, K.H. Kim, H.J. Sung, S. Ahn, Water-soluble binder with high flexural modulus for powder injection molding, Journal of Materials Science 40 (5) (2005) 1105–1109.
[29] M. Zaky, Effect of solvent debinding variables on the shape maintenance of green molded bodies, Journal of Materials Science 39 (10) (2004) 3397–3402.
[30] H.-K. Lin, K.-S. Hwang, In situ dimensional changes of powder injection-molded compacts during solvent debinding, Acta Materialia 46 (12) (1998) 4303–4309.
[31] W. Liu, X. Yang, Z. Xie, C. Jia, L. Wang, Novel fabrication of injection-moulded ceramic parts with large section via partially water-debinding method, Journal of the European Ceramic Society 32 (10) (2012) 2187–2191.
[32] M.D. Abràmoff, P.J. Magalhães, S.J. Ram, Image processing with imagej, Biophotonics International 11 (7) (2004) 36–42.
[33] D.-S. Tsai, W.-W. Chen, Solvent debinding kinetics of alumina green bodies by powder injection molding, Ceramics International 21 (4) (1995) 257–264.
[34] D. Blattner, M. Kolb, H. Leuenberger, Percolation theory and compactibility of binary powder systems, Pharmaceutical Research 7 (2) (1990) 113–117.
[35] A. Sidambe, I. Figueroa, H. Hamilton, I. Todd, Metal injection moulding of CP-Ti components for biomedical applications, Journal of Materials Processing Technology 212 (7) (2012) 1591–1597.
[36] S. Grandi, A. Magistris, P. Mustarelli, E. Quartarone, C. Tomasi, L. Meda, Synthesis and characterization of SiO_2-peg hybrid materials, Journal of Non-crystalline Solids 352 (3) (2006) 273–280.